Design of double-bend and multibend achromat lattices with large dynamic aperture and approximate invariants

Yongjun Li,[1,*] Kilean Hwang,[2,3] Chad Mitchell,[3,†] Robert Rainer,[1]
Robert Ryne,[3] and Victor Smaluk[1]

[1]*Brookhaven National Laboratory, Upton 11973, New York, USA*
[2]*Michigan State University, East Lansing, Michigan 48824, USA*
[3]*Lawrence Berkeley National Laboratory, Berkeley 94720, California, USA*

(Received 7 August 2021; accepted 23 November 2021; published 27 December 2021)

A numerical method to design nonlinear double- and multibend achromat (DBA and MBA) lattices with approximate invariants of motion is investigated. The search for such nonlinear lattices is motivated by Fermilab's Integrable Optics Test Accelerator, whose design is based on an integrable Hamiltonian system with two invariants of motion. While it may not be possible to design an achromatic lattice for a dedicated synchrotron light source storage ring with one or more exact invariants of motion, it is possible to tune the sextupoles and octupoles in existing double- and multibend achromat lattices to produce approximate invariants. In our procedure, the lattice is tuned while minimizing the turn-by-turn fluctuations of the Courant-Snyder actions J_x and J_y at several distinct amplitudes, while simultaneously minimizing diffusion of the on-energy betatron tunes. The resulting lattices share some important features with integrable ones, such as a large dynamic aperture, trajectories confined to invariant tori, robustness to resonances and errors, and a large amplitude-dependent tune spread. Compared to the nominal National Synchrotron Light Source-II lattice, the single- and multibunch instability thresholds are increased and the bunch-by-bunch feedback gain can be reduced.

DOI: 10.1103/PhysRevAccelBeams.24.124001

I. INTRODUCTION

The Integrable Optics Test Accelerator (IOTA) [1], whose design is based on an integrable Hamiltonian system with two invariants of motion [2,3], paves the way for a new class of highly nonlinear storage rings. Experiments using a lattice design with one invariant of motion have also been performed, both at IOTA and in the University of Maryland Electron Ring [4]. In each case, the lattice is tuned to provide one or more analytically known invariants of motion, resulting in a dynamic aperture (DA) that is large and robust to the presence of resonances.

The storage rings used as dedicated synchrotron light sources are designed in a different way: a linear achromat lattice with a desired beam emittance is designed first, and then the nonlinear dynamics is optimized with sextupoles and/or octupoles. The nonlinear magnets are often tuned to control the low-order resonance driving terms of the one-turn map [5] to obtain sufficient DA. Under these conditions it is generally difficult, if not impossible, to optimize the nonlinear dynamics to produce a one-turn map with one or more exact invariants. However, it is sometimes possible to produce approximate invariants, or quasi-invariants (QI), in these achromat lattices. This paper describes a procedure for designing near-integrable double-bend achromat (DBA) and multibend achromat (MBA) lattices with two QI. The motivation for constructing such lattices is that, although they are not completely integrable, the DA is large and robust to the presence of resonances. While crossing the resonance lines, their stop-band widths are observed to be narrow. Like nonlinear integrable lattices such as the one at IOTA, these lattices also have a large amplitude-dependent betatron tune-spread which can increase instability and space charge thresholds due to improved Landau damping [6,7]. As a result, the requirements on the feedback system's gain can be reduced significantly. This research was motivated by related studies such as the square matrix method [8] and the constant Courant-Snyder invariant method [9,10].

The remainder of this paper is outlined as follows: Sec. II explains the concept of Poisson-commuting invariants in integrable Hamiltonian systems, and describes a numerical approach for optimizing the nonlinear lattice to produce approximate invariants using symplectic tracking.

*yli@bnl.gov
†chadmitchell@lbl.gov

Sections III and IV describe the properties of two such lattices, both of which have been constructed: the existing National Synchrotron Light Source-II (NSLS-II) DBA storage ring and a diffraction-limited MBA storage ring (whose design is preliminary). Some detailed studies of the DBA lattice are described in Sec. V. Section VI describes the simulation of a kicked beam to illustrate the decoherence effect that results from a large nonlinear tune spread. Some discussion and a brief summary are given in Sec. VII. A technique to modify the action-like invariants to reshape the invariant tori (and the resulting DA) is described in the Appendix.

II. LATTICE DESIGN PROCEDURE

A Hamiltonian system is Liouville integrable if it possesses a maximal set of independent Poisson commuting invariants of motion. For a system described by a symplectic map on a phase space of dimension $2n$, this means that there exist n functions f_j $(j = 1, \ldots, n)$ on the phase space such that (i) each f_j is invariant under the map, (ii) the Poisson brackets satisfy $[f_i, f_j] = 0$, and (iii) the set of gradient vectors $\{\nabla f_j : j = 1, \ldots, n\}$ is linearly independent [11,12]. The behavior of trajectories for a completely integrable system is well known, i.e., all its trajectories are confined to tori with well-defined and stable tunes.

By ignoring radiation and longitudinal acceleration, a charged particle's transverse motion in a storage ring is a four-dimensional Hamiltonian system, described by a symplectic one-turn map $\mathcal{M}$. If we let the canonical coordinates of the system be denoted $z = (x, p_x; y, p_y)$, a quantity $f(z)$ is an invariant of the map $\mathcal{M}$ if

$$f(\mathcal{M}(\mathbf{z})) = f(\mathbf{z}). \tag{1}$$

If two such invariants f_i, $(i = 1,\ 2)$ exist, if they are independent

$$\nabla f_1 \times \nabla f_2 \neq 0, \tag{2}$$

and if they Poisson commute

$$[f_1, f_2] = \left(\frac{\partial f_1}{\partial x}\frac{\partial f_2}{\partial p_x} - \frac{\partial f_1}{\partial p_x}\frac{\partial f_2}{\partial x}\right) + \left(\frac{\partial f_1}{\partial y}\frac{\partial f_2}{\partial p_y} - \frac{\partial f_1}{\partial p_y}\frac{\partial f_2}{\partial y}\right) = 0, \tag{3}$$

the lattice is Liouville integrable.

When the map $\mathcal{M}$ is linear and uncoupled, the Courant-Snyder actions J_x and J_y form the most commonly used Poisson commuting pair of invariants, where

$$J_x = \frac{1}{2}(\bar{x}^2 + \bar{p}_x^2) = \frac{1}{2}(\gamma_x x^2 + 2\alpha_x x p_x + \beta_x p_x^2), \tag{4}$$

in the horizontal plane, with a similar expression for J_y. Here α_x, β_x, and γ_x are the horizontal Twiss parameters [13] at the longitudinal location where the Poincaré section is observed. The canonical action-angle coordinates are $(\Phi_x, J_x, \Phi_y, J_y)$, where $\Phi_{x,y}$ denotes the betatron phase in each plane, and the one-turn map is determined by the phase advance completed in a single revolution:

$$\begin{aligned}\phi_x &= \Phi_{x,i+1} - \Phi_{x,i} \\ &= -\arctan\left(\frac{\bar{p}_{x,i+1}}{\bar{x}_{i+1}}\right) + \arctan\left(\frac{\bar{p}_{x,i}}{\bar{x}_i}\right) + k \cdot 2\pi,\end{aligned} \tag{5}$$

with a similar expression for ϕ_y. Here, k is the integer part of the betatron tune. The phase advance values ϕ_x, ϕ_y are independent of the actions J_x and J_y.

In a realistic storage ring, once the linear lattice and the nonlinear magnet locations are fixed, the one-turn map $\mathcal{M}$ depends on the nonlinear magnet strengths K_i, with $i \geq 2$. It is difficult, if not impossible, to tune the K_i so that $\mathcal{M}$ possesses even one exact invariant. However, we can imitate the linear case by constructing a nonlinear system in which the Courant-Snyder actions J_x, J_y form a pair of approximate invariants, as illustrated in Fig. 1. Unlike the linear case, however, the phase advance values ϕ_x and ϕ_y can depend on the actions J_x and J_y.

The procedure is as follows. To optimize the behavior of the Courant-Snyder action J_x within the available DA, multiple particles with different values of $J_{x,0}$ are launched. Element-by-element tracking of this set of particles is used to compute the turn-by-turn evolution of J_x. The tracking is implemented with a kick-drift symplectic integrator [14] to

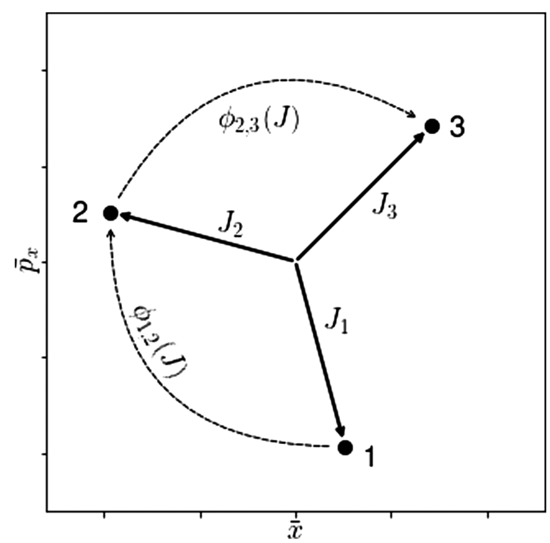

FIG. 1. Schematic illustration of a rotating trajectory observed at a Poincaré section with normalized coordinates $(\bar{x}, \bar{p}_x)$. The fluctuations of the action J_x and phase advance ϕ_x observed in multiturn tracking simulations are the objectives to be minimized. A similar picture applied in the vertical plane.

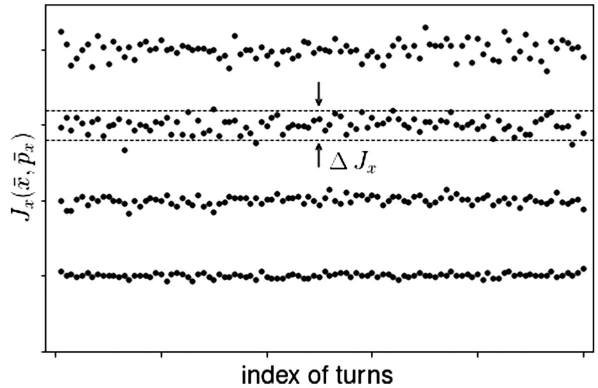

FIG. 2. Schematic illustration of the fluctuation of actions ΔJ_x starting from different initial amplitudes. Usually the fluctuations increase gradually with the initial amplitude.

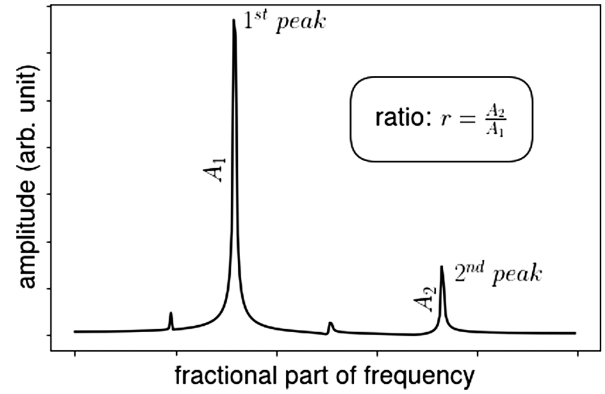

FIG. 3. Schematic illustration of the spectrum obtained from turn-by-turn trajectory data $\bar{x} \pm i\bar{p}_x$. The ratio between the amplitudes of the two leading frequencies $\frac{A_2}{A_1}$ is the objective to be minimized to suppress the orbit tune diffusion.

preserve the geometry of the Hamiltonian system. The available nonlinear knobs are simultaneously tuned to minimize the turn-by-turn fluctuations of J_x for each particle, as illustrated in Fig. 2.

At the same time, we minimize the turn-to-turn variations of the horizontal phase advance. Instead of directly calculating the phase advance for each turn with Eq. (5), the complex turn-to-turn evolution of $\bar{x} \pm i\bar{p}_x$ [15] was analyzed in the frequency domain. One reason for using such a spectral method is to determine whether the fractional tune is below or above the half integer. The amplitudes of the two leading frequencies were computed utilizing the Numerical Analysis of Fundamental Frequencies (NAFF) technique [16]. By tuning the nonlinear knobs, the ratio between the two leading frequencies $r = \frac{A_2}{A_1}$ was minimized. As a consequence, the smaller amplitude frequencies were also suppressed (Fig. 3). In principle, the summation of all non-fundamental peaks should be compared against the fundamental frequency peak, but the computational cost will become high. Since NAFF outputs the peaks in descending order, we only use the two leading peaks to get a quick but rough approximation. This procedure is performed independently for several initial conditions of varying amplitude. As a result, the tune diffusion of each particle is suppressed, but the tunes may be amplitude-dependent. The same procedure is repeated for the vertical plane.

Since the goal is to minimize the fluctuations of four different quantities for different initial conditions simultaneously, the construction of such a nonlinear lattice becomes a typical multiobjective optimization problem: (i) given a set of nonlinear knobs K_i within their allowed ranges; (ii) subject to some constraints, such as maintaining certain desired chromaticities; (iii) simultaneously minimize the objective functions, i.e., $\frac{\Delta J_{x,y}}{J_{x,y}}$ and $r_{x,y} = \frac{A_{2;x,y}}{A_{1;x,y}}$ of multiparticles launched from different initial conditions.

Multiobjective optimization techniques are now widely used in the accelerator community. Here, the nondominated sorting genetic algorithm (NSGA-II) [17] was used. Five virtual particles with gradually increasing initial values of $J_{0;x,y}$ were launched, and for each initial condition, four objectives were used. The total number of objectives was therefore $5 \times 4 = 20$.

Thus far, we have only discussed uncoupled linear lattices. When linear coupling is present, a different parameterization, such as the one described in Ref. [18], is needed.

III. APPLIED TO DOUBLE-BEND ACHROMAT

In this section, we introduce a nonlinear DBA lattice for the NSLS-II main storage ring [19], which is presently in operation at Brookhaven National Laboratory. It is a third generation medium energy (3 GeV) light source. The storage ring's lattice is a typical DBA structure with its main parameters listed in Table I. Its linear optics for one cell is illustrated in Fig. 4. The whole ring is composed of 30 such cells. In this configuration, three families of chromatic sextupoles are used to correct its chromaticity to $+7$. Then, six families of harmonic sextupoles in dispersion-free sections are used as tuning knobs for the multiobjective optimization described in Sec. II.

Below, we present the nonlinear lattice performance of an optimized solution using the tracking simulation code ELEGANT [20]. All the tracking simulations in this paper were performed with this code unless stated otherwise.

TABLE I. Main parameters of NSLS-II storage ring.

Parameters	Values
Horizontal emittance (nm)	2.1
Natural chromaticity (x/y)	$-101/-40$
Tune (x/y)	33.22/16.26
Energy spread	5.1×10^{-4}
Damping partition $(x/y/s)$	1.0/1.0/2.0

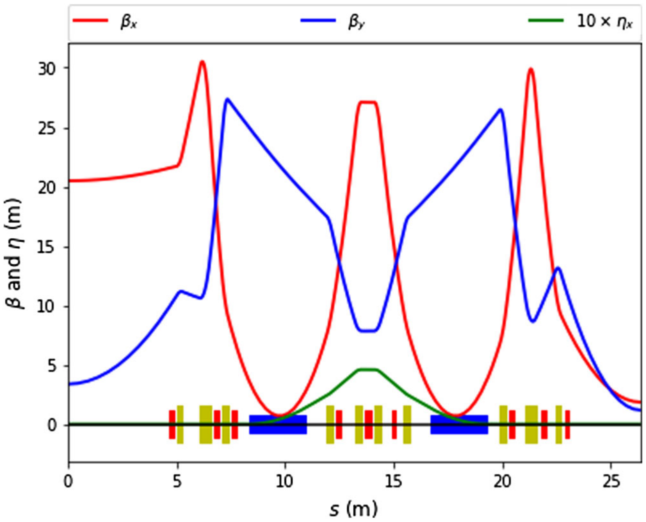

FIG. 4. Linear optics and magnet layout for one cell of the NSLS-II storage ring. The red blocks represent sextupoles. The strengths of six harmonic sextupoles were tuned during optimization of the nonlinear optics (Sec. II).

Figure 5 illustrates on-momentum DA (through 1,024 turns of particle tracking) observed at the center of the long straight section, i.e., $s = 0$ in Fig. 4. Each stable initial condition is colored with its tune diffusion $\log_{10}(\Delta\nu_x^2 + \Delta\nu_y^2)$ [16] obtained from turn-by-turn data using the NAFF algorithm. The nominal operation lattice's DA at chromaticity $\xi = 2$ is also shown for comparison. Although stronger sextupoles are needed to correct the chromaticity in the QI lattice, the obtained DA is comparable with the nominal operation lattice.

The turn-by-turn evolution of the Courant-Snyder actions $J_{x,y}$ for particles at five distinct amplitudes are shown in Fig. 6. The size of the visible fluctuations increases gradually with the amplitude of the initial condition. The spectral analysis of tracking data using the NAFF technique indicates that some nondominant frequencies gradually become stronger as well. The amplitude ratio between the two leading frequencies increases as shown in Fig. 7.

One of the features of an integrable system is that the trajectories are confined to tori in the phase space. This is

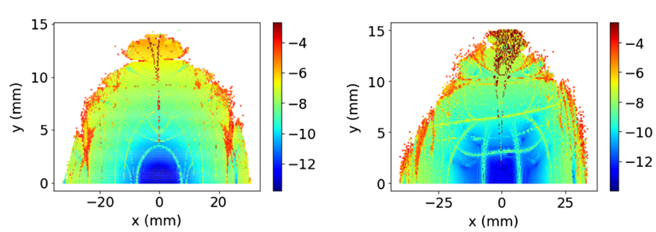

FIG. 5. DA of the DBA lattice with QI (left) and the NSLS-II lattice at nominal operation (right). The lattices have chromaticities of $\xi = 7$ and $\xi = 2$, respectively. Colors indicate the tune diffusion obtained with the NAFF technique.

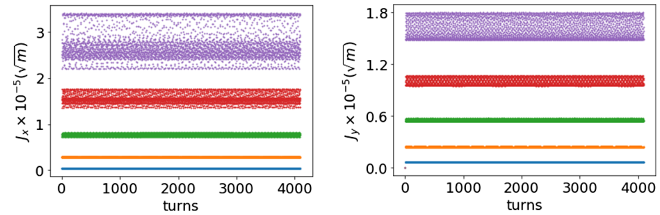

FIG. 6. Evolution of $J_{x,y}$ in the DBA lattice starting from five different initial conditions in the horizontal (left) and vertical (right) planes.

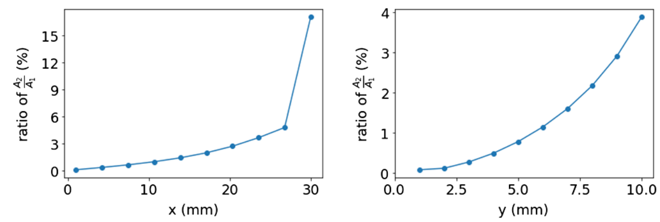

FIG. 7. Ratio of the two leading NAFF components increases with the initial particle amplitude in the horizontal (left) and vertical (right) planes for the DBA lattice.

apparent in the turn-by-turn tracking data shown in Fig. 8. Although trajectories begin to gradually deviate from the Courant-Snyder ellipse when the amplitude increases, they are still confined to deformed tori. It therefore appears that this lattice possesses two QIs whose values near the reference orbit are quantitatively close to the Courant-Snyder actions. This feature can also be observed from the symmetry of DA in the horizontal plane as shown in Fig. 5.

Like the IOTA ring, this lattice also provides a large amplitude-dependent tune-spread as illustrated in the left subplot of Fig. 9. This property can increase instability and space charge thresholds through improved Landau damping. Even while crossing the low-order resonance lines such as $\nu_x = 1/3$, the stop-band widths are observed to be much narrower than those in conventional nonlinear lattices [21,22]. The nominal operation lattice's tune

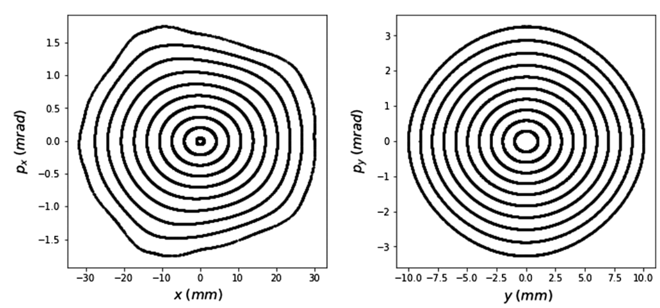

FIG. 8. Simulated trajectories of the DBA lattice starting from different initial conditions in the horizontal (left) and vertical (right) phase space. Within the DA, although the trajectories deviate from the Courant-Snyder ellipse, they are still confined to thin tori.

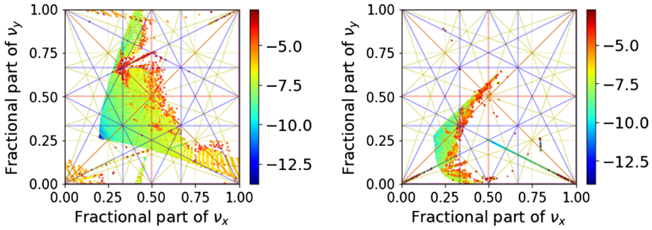

FIG. 9. Tune footprint of the NSLS-II DBA lattice with QI (left) and the nominal lattice for routine operation (right). The design working point is 33.22/16.26. Compared to the nominal lattice, a very large amplitude-dependent tune-spread is observed in the QI lattice, and various resonance lines can be crossed with narrow stop-band widths. Here colors indicate the tune diffusion, as in Fig. 5.

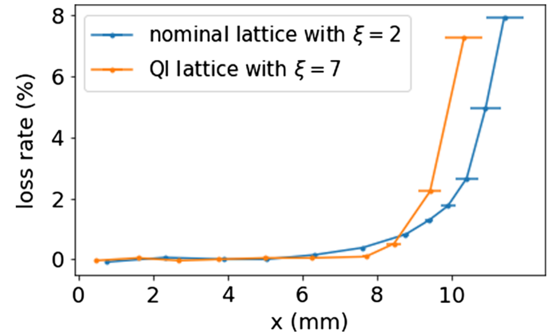

FIG. 11. Measured dynamic aperture of the DBA lattice with QI (yellow) and the NSLS-II lattice at nominal operation (blue). The lattice chromaticities are $\xi = 7$ and $\xi = 2$, respectively.

footprint (as shown in the right subplot) can provide a smaller tune spread within the bunch when an instability occurs.

It is interesting to directly compare the fluctuations in actions for the QI lattice and the nominal lattice. Although their DAs are comparable, the fluctuations ΔJ in the QI lattice are better suppressed as illustrated in Fig. 10. When a small physical aperture exists in a ring, such as an undulator's gap, a trajectory with large action variation might be blocked. Then its realistic DA will be smaller than the physical aperture. In this case, a less fluctuating trajectory will be preferable.

The robustness of this lattice has been confirmed with a beam test. After loading its sextupoles settings, a near 100% off axis injection efficiency was achieved, which indicates its DA is sufficient for routine operation. Then, the horizontal DA was scanned by kicking the beam transversely to observe its loss rate as shown in Fig. 11. Although the measured DA is about 10 ± 1 mm, which is worse than the simulation prediction due to various realistic errors, it still can satisfy the requirement (>8.5 mm) for off axis injection. The nominal operation lattice's DA is also shown for comparison.

A bunch-by-bunch feedback (BBFB) system is frequently used in light source rings to suppress instabilities in the beam centroid motion. Limiting the BBFB gain is

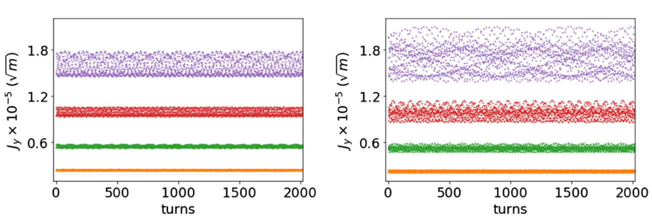

FIG. 10. Comparison of the vertical action fluctuations in the QI lattice (left) and the nominal NSLS-II lattice (right). Starting from the same initial conditions (x, p_x, y, p_y), the action in the QI lattice has smaller fluctuations, despite the fact that the lattice has a high chromaticity $\xi = 7$. The same feature can also be observed for the horizontal plane.

critical to avoid a degradation of the beam brightness. For example, a significant vertical emittance increase was observed when an excess gain was applied [23] at the NSLS-II ring. Although the beam centroid instabilities could be well suppressed with the BBFB system, the emittance blowup effect due to a large feedback gain was pronounced, especially at higher chromaticity.

In this study, after accumulating a beam current of 400 mA, the BBFB system was reoptimized to reduce its gain gradually. Each bunch's turn-by-turn data was used for a spectral analysis to identify the appearance of sidebands of betatron motion caused by various instabilities. Compared with the NSLS-II lattice at nominal operation, the required gain for the nonlinear QI lattice was reduced by 50% and 75% in the horizontal and vertical planes, respectively. This appears to be due to the increase in nonlinear tune-spread and chromaticity.

The single bunch instability threshold was also increased in the QI lattice. For the nominal lattice, the charge threshold is around 2–3 mA without using BBFB, and 5–6 mA with BBFB [24]. For the QI lattice, this threshold was observed to be greater than 8 mA without BBFB, and 12 mA with BBFB. The actual threshold might be higher, because the single bunch accumulation was interrupted by high outgassing due to the extensive single bunch radiation pulse.

IV. APPLIED TO MBA

Low-emittance light source ring design is now entering a new era. Various MBA-type lattices already reach diffraction-limited horizontal emittances to deliver much brighter X-ray beams. Like the DBA case, it is interesting to explore whether it is possible to design a nonlinear MBA lattice with two QIs. The ESRF-EBS type hybrid MBA lattice [25] has been widely adopted by other facilities. It is also being considered as one of the options for future NSLS-II brightness upgrade. A preliminary 7-BA design is shown in Fig. 12, which illustrates the linear optics for one cell. Note that several reverse bends are incorporated [26,27]. The main parameters are listed in Table II.

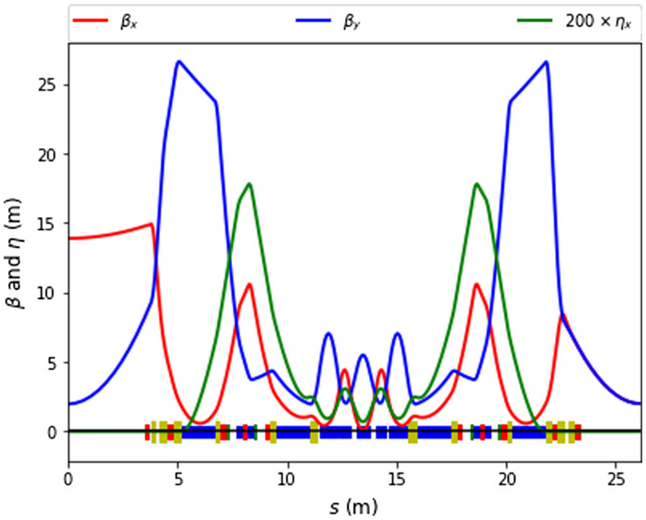

FIG. 12. Linear optics and magnet layout for one cell of an ESRF-EBS type hybrid 7BA lattice. The red blocks represent sextupoles. Six chromatic sextupoles grouped into five families inside two dispersive bumps are used to correct the chromaticity with three extra degrees of freedom. Four harmonic sextupoles and four dispersive octupoles (green blocks) are also available for nonlinear dynamics optimization.

A two-stage optimization has been implemented. First, the settings of the chromatic and harmonic sextupoles were optimized to correct the chromaticities, to minimize the fluctuations of the Courant-Snyder actions, and to maximize the ratio of the two leading frequency components. After this procedure, four octupoles inside the dispersive bumps were optimized to further minimize these objectives. The resulting DA is shown in Fig. 13.

The MBA lattice was found to be more challenging than the DBA lattice in constructing QI. The Courant-Snyder actions have larger fluctuations after optimization, especially in the vertical plane. Nevertheless, particle orbits are still confined to tori in the horizontal plane, as seen in Fig. 14. More importantly, a large amplitude-dependent tune-spread is observed within the tune footprint of the stable DA, as shown in Fig. 15.

At large amplitudes, the trajectories in the vertical phase space significantly deviate from the Courant-Snyder ellipse (Fig. 14). However, this does not necessarily indicate that the tori are broken, as the two-dimensional projections of four-dimensional tori are observed. A more detailed analysis, for example, expanding the QI expression to high-order polynomials for large-amplitude orbits in the vertical plane might be considered needed.

TABLE II. Main parameters of the test hybrid MBA ring.

Parameters	Values
Horizontal emittance (pm)	31
Natural chromaticity (x/y)	$-125/-108$
Tune (x/y)	73.19/28.62
Energy spread	7.1×10^{-4}
Damping partition $(x/y/s)$	2.0/1.0/1.0

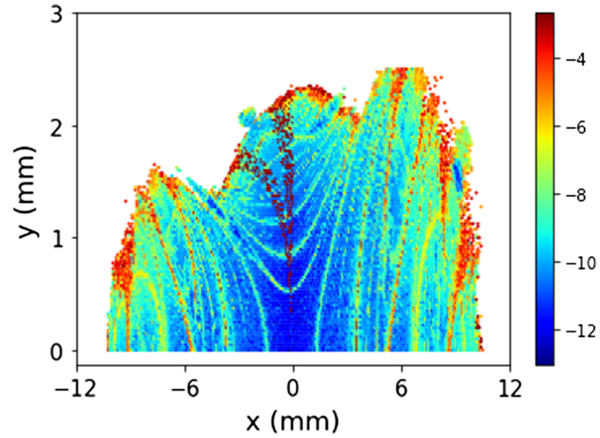

FIG. 13. DA of the MBA lattice in the transverse $x-y$ plane colored with the tune diffusion.

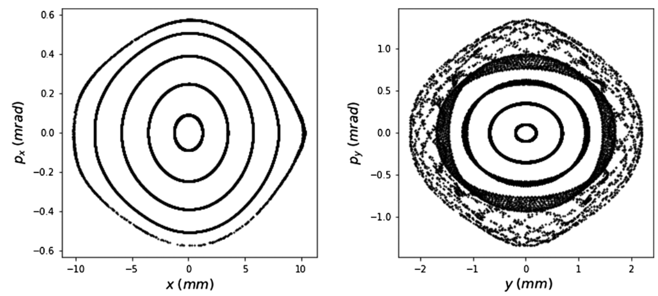

FIG. 14. Simulated trajectories of the MBA lattice in the horizontal (left) and vertical (right) phase space. The vertical trajectories begin to smear out from thin tori gradually, but some patterns are visible.

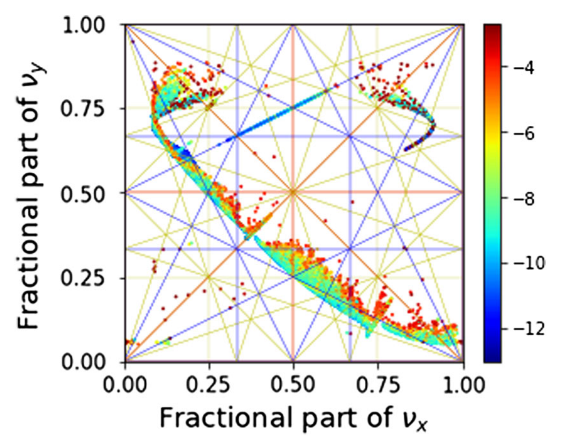

FIG. 15. Large amplitude-dependent tune spread is observed in the MBA lattice constructed with QI.

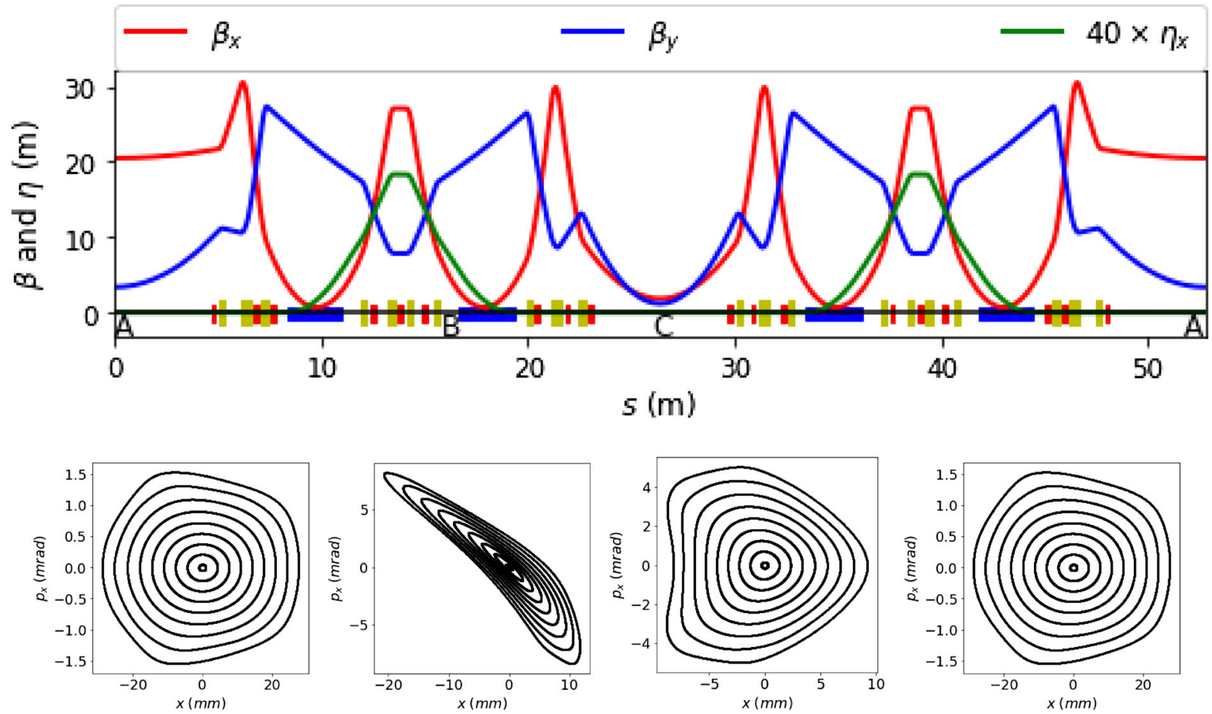

FIG. 16. Tori are near-circular only when observed at the long straight centers but could be distorted at other locations. The bottom four subplots are the tori observed at the locations "A-B-C-A," respectively, as marked in the top subplot.

V. DEPENDENCE ON LATTICE LOCATION

In the previous examples, the optimization procedure of Sec. II was performed using tracking data at a specific lattice location, e.g., at the center of the straight section. Here, the orbits lie on invariant tori that are nearly circular when projected into the $\bar{x} - \bar{p}_x$ and $\bar{y} - \bar{p}_y$ planes. However, it is not surprising to observe that the invariant tori are distorted at other locations in the lattice. Figure 16 shows an example of distorted tori observed at a location inside an achromat of the NSLS-II DBA lattice. The one-cell map behaves like an "optical anastigmat", which has circular tori only at the periodic locations, i.e., its entrance and exit. Elsewhere in the lattice, distorted (perhaps broken) tori can be observed.

VI. DECOHERENCE DUE TO NONLINEARITY

At the IOTA ring, its large amplitude-dependent tune spread was found to provide a stabilization mechanism due to improved Landau damping [28]. Since constructed lattices with QI also provide a large nonlinear amplitude detuning, we used the DBA lattice to implement a four-dimensional multiparticle simulation to illustrate this nonlinearity. A large tune spread due to the nonlinearity of betatron oscillations can be indirectly observed by kicking a bunched beam transversely [29]. A Gaussian distributed bunched beam was simulated by 2000 macroparticles with the horizontal beam size σ_x. After being kicked to an amplitude $Z = a\sigma_x$, the beam centroid will decay to the origin as the betatron phases of particles at different amplitudes decohere, which is described by the decoherence factor,

$$A(N) = \frac{1}{1+\theta^2} \exp\left[-\frac{Z^2}{2}\frac{\theta}{1+\theta^2}\right]. \tag{6}$$

Here, N is the number of turns after being kicked, $\theta = 4\pi\mu N$, and $\mu(Z) = \frac{d\nu}{da^2}$ is the local amplitude detuning coefficient at Z. The phase-space distribution of the beam filaments from a localized bunch to an annulus which occupies all betatron

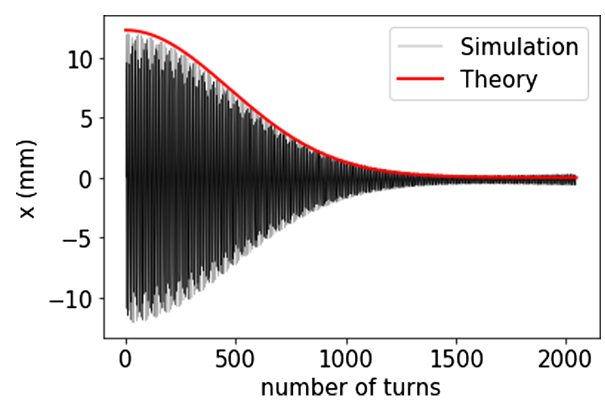

FIG. 17. After being kicked, the centroid of the beam will show a decaying oscillation. The red line is known as the decoherence factor in Eq. (6) and can be used to determine the local amplitude detuning coefficient μ.

phases and the observed centroid of the beam will show a decaying oscillation as seen in Fig. 17. From the decoherence factor curve (the red line in Fig. 17), the local tune-shift-with-amplitude coefficient can be determined and confirmed to be consistent with the spectrum analysis of the single particle tracking data.

VII. DISCUSSION AND SUMMARY

So far, only the on-momentum particle motion has been described. In practice, a sufficient off-momentum acceptance is required as well. In the two examples of Secs. III and IV, on-momentum lattices were constructed with two quasi-invariants, and then the off-momentum acceptances were checked with tracking simulations. Both lattices were found to have sufficient local momentum aperture for the Touschek lifetime as shown in Fig. 18. In case the momentum acceptance also needs to be optimized, the method can be expanded to include a set of off-momentum particles. For an off-momentum particle, the dispersive reference orbit needs to be computed first, and then the Courant-Snyder actions $J_{x,y}$ in Ref. (4) need to be computed using the momentum-dependent Twiss parameters $\alpha(\delta, K_i), \beta(\delta, K_i)$, and $\gamma(\delta, K_i)$. Note that the momentum-dependent Twiss parameters depend on the nonlinear magnets' excitation values K_i. For a given nonlinear magnet setting, the reference closed orbit and the corresponding momentum-dependent Twiss parameters need to be updated prior to the normalization.

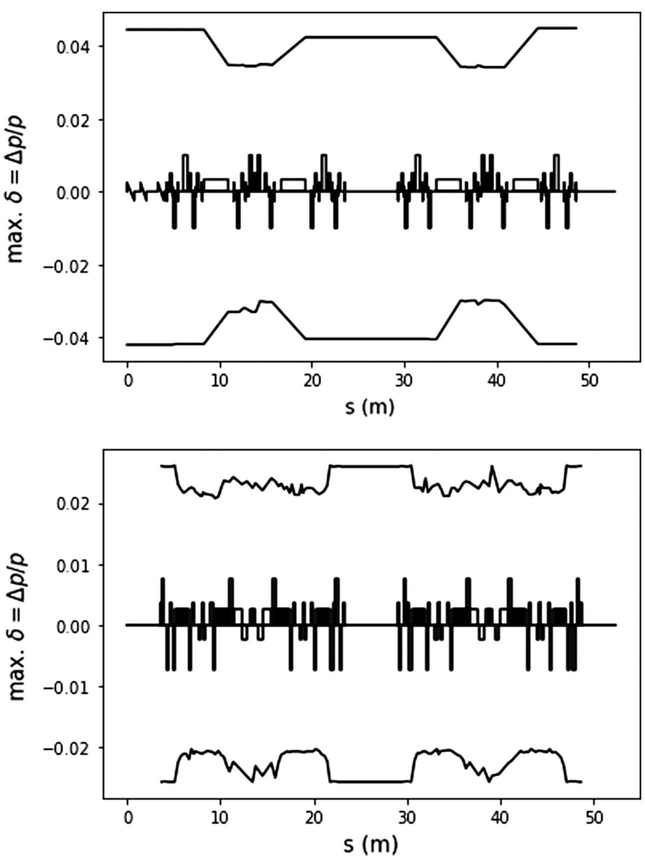

FIG. 18. Local momentum aperture of one supercell (including two mirror symmetric cells) for the constructed DBA (top) and MBA (bottom) lattices.

In this paper, we demonstrated that a conventional DBA or MBA lattice can be retuned to possess two approximate invariants by optimizing the settings of only the sextupoles and octupoles. While the resulting DA is large (but finite), most particle trajectories are regular and confined to tori, and the amplitude-dependent betatron tunes are well defined and stable. Like the lattice of the IOTA ring, a large nonlinear tune spread exists that can provide enhanced Landau damping. The stop-band widths are observed narrow while the tune crosses low-order resonance lines.

ACKNOWLEDGMENTS

We would like to thank L-H. Yu, B. Bacha, X. Yang, and other NSLS-II colleagues for the stimulating discussion and/or productive experimental studies, M. Borland, R. Lindberg, Y-P. Sun, W. Cheng (ANL) and Y. Hao (MSU), E. Stern, A. Valishev, A. Romanov (FNAL), N. Kuklev (UChicago), G. Xu (IHEP) for the stimulating and collaborative discussions. This research is supported by the U.S. Department of Energy (DoE) under Contract No. DE-SC0012704 (BNL) and DE-AC02-05CH11231 (LBNL). Co-authors from LBNL would like to acknowledge the support from the U.S. DoE Early Career Research Program under the Office of High Energy Physics.

APPENDIX: ALTERNATIVE OPTIMIZATION SCHEMES

We can add additional terms to the Courant-Snyder actions $J_{x,y}$ in Ref. (4), and use these in the optimization procedure described in Sec. II, in order to construct a lattice with more complicated quasi-invariants. Here, we demonstrate this method by modifying the quasi-invariant J_x to obtain triangle-shaped tori,

$$\begin{aligned} J_x(\phi_x) &= J_0 + \Delta J_x(\phi_x) \\ &= J_0\left\{1 + \delta \sin\left[n\left(\phi_x - \frac{\pi}{2n}\right)\right]\right\}, \end{aligned} \tag{A1}$$

where $\delta = \frac{\Delta J_x}{J_x}$ and $n = 3$. The phase dependence (top) of J_x and the expected torus in the horizontal phase space (bottom) are illustrated in Fig. 19.

After modifying the optimization procedure to minimize the fluctuations of Eq. (A1) in the DBA lattice, a new set of sextupole settings were obtained. Tracking simulation confirmed that the tori have been reshaped as expected (Fig. 20). Such a phase space manipulation technique might be useful when a nonsymmetric DA is desired. For example, a slightly larger inboard DA might

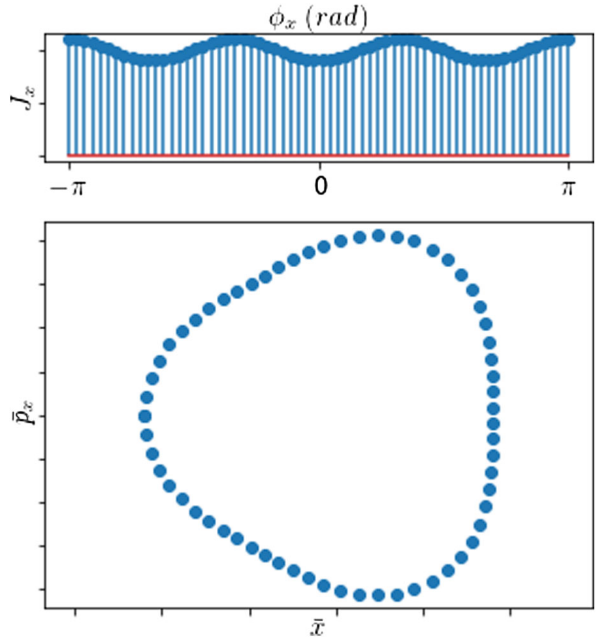

FIG. 19. Adding a periodic phase dependence (top) to the action J_x can reshape a circular torus into a triangle-shaped one (bottom).

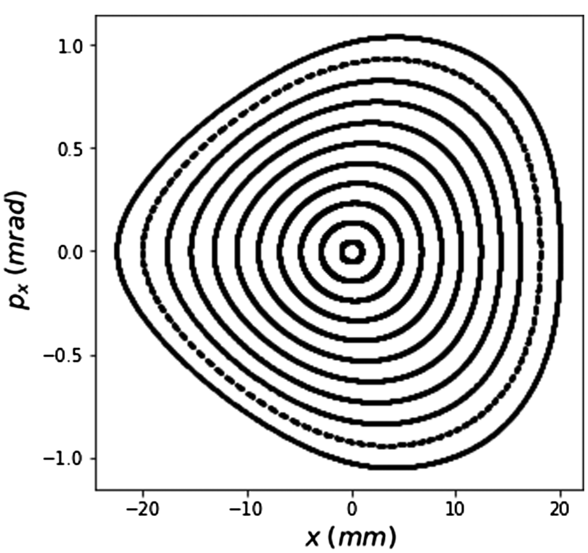

FIG. 20. Particle trajectories are confined to triangle-shaped tori, as confirmed by the tracking simulation. A nonsymmetric DA can be obtained with this technique.

be preferred to capture off axis injected beams from that region.

However, the phase dependence of Eq. (A1) can introduce additional frequency components into the betatron spectrum. For example, a weak component sitting near $1/3$ is visible through the NAFF analysis. If the betatron phase dependence is weak, it does not appear to spoil the overall performance of the nonlinear lattice. Note that the triangle-shaped tori are not caused by the betatron tune's approaching a third-order resonance, because the main betatron tune is around 0.22, and still far away from $1/3$.

[1] S. Antipov, D. Broemmelsiek, D. Bruhwiler, D. Edstrom, E. Harms, V. Lebedev, J. Leibfritz, S. Nagaitsev, C. S. Park, H. Piekarz, P. Piot, E. Prebys, A. Romanov, J. Ruan, T. Sen, G. Stancari, C. Thangaraj, R. Thurman-Keup, A. Valishev, and V. Shiltsev, IOTA (integrable optics test accelerator): Facility and experimental beam physics program, J. Instrum. **12**, T03002 (2017).
[2] V. Danilov, Practical solutions for nonlinear accelerator lattice with stable nearly regular motion, Phys. Rev. ST Accel. Beams **11**, 114001 (2008).
[3] V. Danilov and S. Nagaitsev, Nonlinear accelerator lattices with one and two analytic invariants, Phys. Rev. ST Accel. Beams **13**, 084002 (2010).
[4] K. Ruisard, H. B. Komkov, B. Beaudoin, I. Haber, D. Matthew, and T. Koeth, Single-invariant nonlinear optics for a small electron recirculator, Phys. Rev. Accel. Beams **22**, 041601 (2019).
[5] A. Dragt, Lie methods for nonlinear dynamics with applications to accelerator physics (to be published), https://www.physics.umd.edu/dsat/dsatliemethods.html.
[6] A. Chao, *Physics of Collective Beam Instabilities in High Energy Accelerators* (Wiley, New York, 1993).
[7] E. Stern, Suppression of instabilities generated by an anti-damper with a nonlinear magnetic element in IOTA, Technical Report No. FERMILAB-CONF-18-132-APC-CD, Fermi National Accelerator Laboratory, 2018.
[8] L. Yu, Analysis of nonlinear dynamics by square matrix method, Phys. Rev. Accel. Beams **20**, 034001 (2017).
[9] M. Borland (private communication).
[10] Y. Sun and M. Borland, Comparison of nonlinear dynamics optimization methods for APS-U, in *Proceedings of 2nd North American Particle Accelerator Conference* (2017), p. WEPOB15.
[11] J. Liouville, Note sur l'intégration des équations différentielles de la dynamique, présentée au bureau des longitudes le 29 juin 1853, Journal de Mathématiques pures et appliquées, 137 (1855), https://eudml.org/doc/233980.
[12] V. Arnold, *Mathematical Methods of Classical Mechanics* (Springer–Verlag, Berlin and New York, 1989).
[13] E. Courant and H. Snyder, Theory of the alternating-gradient synchrotron, Ann. Phys. (Leipzig) **3**, 1 (1958).
[14] H. Yoshida, Construction of higher order symplectic integrators, Phys. Lett. A **150**, 262 (1990).
[15] A. Chao, *Lecture Notes on Topics in Accelerator Physics* (SLAC, Stanford, CA, 2002).
[16] J. Laskar, Frequency map analysis and particle accelerators, in *Proceedings of 20th Particle Accelerator Conference (PAC 03)* (Portland, 2003), p. 378.
[17] K. Deb, *Multi-Objective Optimization Using Evolutionary Algorithms* (Wiley, New York, 2001).
[18] D. Edwards and L. Teng, Parametrization of linear coupled motion in periodic systems, IEEE Trans. Nucl. Sci. **20**, 885 (1973).

[19] BNL, https://www.bnl.gov/isd/documents/75003.pdf.

[20] M. Borland, Elegant: A flexible SDDS-compliant code for accelerator simulation, in *Advanced Photon Source LS-287* (Lemont, 2000).

[21] A. Schoch, Theory of non-linear perturbations of betatron oscillations, CERN, Geneva, Report No. 57, 1957.

[22] H. Wiedemann, *Resonances. In: particle accelerator physics* (Springer Nature, New York, 2015).

[23] W. Cheng, B. Bacha, Y. Li, and D. Teytelman, Developments of bunch by bunch feedback system at NSLS-II storage ring, in *Proceedings of 9th International Particle Accelerator Conference* (Vancouver, 2018).

[24] W. Cheng, B. Bacha, G. Bassi, A. Blednykh, B. Podobedov, O. Singh, and V. Smalyuk, Experimental study of single bunch instabilities at NSLS-ii storage ring, in *Proceedings of IPAC16* (Busan, 2016).

[25] L. Farvacque, N. Carmignani, J. Chavanne, A. Franchi, G. Le Bec, S. Liuzzo, B. Nash, T. Perron, and P. Raimondi, A low-emittance lattice for the ESRF, in *Proceedings of IPAC13* (Shanghai, 2013).

[26] B. Riemann and A. Streun, Low emittance lattice design from first principles: Reverse bending and longitudinal gradient bends, Phys. Rev. Accel. Beams **22**, 021601 (2019).

[27] T. Zhang and X. Huang, Numerical optimization of a low emittance lattice cell, Nucl. Instrum. Methods Phys. Res., Sect. A **923**, 55 (2019).

[28] S. Antipov, S. Nagaitsev, and A. Valishev, Single-particle dynamics in a nonlinear accelerator lattice: attaining a large tune spread with octupoles in IOTA, J. Instrum. **12**, P04008 (2017).

[29] R. Meller, A. Chao, J. Peterson, S. Peggs, and M. Furman, Decoherence of kicked beams, Report No. SSC-N-360, 1987.